Quantum Criticality of the Ising-like Screw Chain Antiferromagnet $SrCo_2V_2O_8$ in a Transverse Magnetic Field

Y. Cui,[1] H. Zou,[2] N. Xi,[1] Zhangzhen He,[3,*] Y. X. Yang,[4] L. Shu,[4,5] G. H. Zhang,[1] Z. Hu,[1] T. Chen,[1] Rong Yu,[1] Jianda Wu,[2,†] and Weiqiang Yu[1,‡]

[1]*Department of Physics and Beijing Key Laboratory of Opto-electronic Functional Materials & Micro-nano Devices, Renmin University of China, Beijing 100872, China*

[2]*Tsung-Dao Lee Institute & School of Physics and Astronomy, Shanghai Jiao Tong University, Shanghai 200240, China*

[3]*State Key Laboratory of Structural Chemistry, Fujian Institute of Research on the Structure of Matter, Chinese Academy of Sciences, Fuzhou, Fujian 350002, China*

[4]*State Key Laboratory of Surface Physics, Department of Physics, Fudan University, Shanghai 200433, China*

[5]*Collaborative Innovation Center of Advanced Microstructures, Nanjing 210093, China*

(Received 3 February 2019; revised manuscript received 29 April 2019; published 9 August 2019)

The quantum criticality of an Ising-like screw chain antiferromagnet $SrCo_2V_2O_8$, with a transverse magnetic field applied along the crystalline a axis, is investigated by ultralow temperature NMR measurements. The Néel temperature is rapidly and continuously suppressed by the field, giving rise to a quantum critical point (QCP) at $H_{C_1} \approx 7.03$ T. Surprisingly, a second QCP at $H_{C_2} \approx 7.7$ T featured with gapless excitations is resolved from both the double-peak structure of the field-dependent spin-lattice relaxation rate $1/^{51}T_1$ at low temperatures and the weakly temperature-dependent $1/^{51}T_1$ at this field. Our data, combined with numerical calculations, suggest that the induced effective staggered transverse field significantly lowers the critical fields, and leads to an exposed QCP at H_{C_2}, which belongs to the one-dimensional transverse-field Ising universality.

DOI: 10.1103/PhysRevLett.123.067203

Novel quantum states with exotic excitations can emerge near a quantum phase transition [1–3]. As one prototype for quantum phase transitions and quantum criticality, the one-dimensional transverse-field Ising model (1DTFIM) has been widely investigated [4–12]. In this model, the magnetic order is suppressed by a transverse magnetic field, resulting in an order-disorder quantum phase transition, with the gap closed at a quantum critical point (QCP), H_C. It has been predicted that a quantum E_8 integrable model emerges near the vicinity of the QCP when a weak longitudinal field is applied [8]. The experimental realization of such a QCP is yet challenging because the interchain exchange couplings in real materials usually stabilize the magnetic order at $T > 0$ and mask the genuine 1D quantum criticality. Nonetheless, a 1DTFIM-like QCP hidden in the 3D ordered phase was suggested in the ferromagnetic chain compound $CoNb_2O_6$ [13–15].

Recently, a class of Ising anisotropic antiferromagnetic screw chain compounds $ACo_2V_2O_8$ ($A = \mathrm{Ba, Sr}$) [16,17] has attracted a lot of research attention. In these compounds, the easy axis is along the chain direction (c axis), and the intrachain exchange coupling $J_z \approx 5$–7 meV [18,19]. Both compounds order at fairly low temperatures (about 5 K), which implies the interchain exchange coupling $J' \ll J$ [20–22]. The magnetic order can be suppressed by a transverse field applied in the ab plane [16,17]. Interestingly, the critical field values and the quantum critical behaviors are very different for fields applied along the [100] and the [110] direction [19,23–29]. In $BaCo_2V_2O_8$, separated 3D and 1D QCPs were suggested with field along the [110] direction at $H \gtrsim 20$ T [28]. For the field along the [100] direction, $H_C \sim 10$ T [24], much lower than the H_C along the [110] direction. With the field along the [100] direction, the linear confining potential arising from the interchain correlation at fields below H_C and the paramagnetism at fields above H_C create different topological excitations [26,30]. The critical behavior near H_C is, however, not investigated.

In order to reveal the properties in the critical regime, low-temperature and low-energy probes are desired. Here, we report our susceptibility and ^{51}V NMR measurements on $SrCo_2V_2O_8$ with $H \| a$ and temperatures down to 50 mK. The main results are summarized in the phase diagram of Fig. 1. From the double-peak signature of the $1/^{51}T_1$ data, we identify two QCPs at $H_{C1} \approx 7$ T and $H_{C2} \approx 7.7$ T, respectively. By analyzing the NMR line splitting at low temperatures, we show that the system establishes three dimensional (3D) magnetic ordering below H_{C1} and the paramagnetic phase above H_{C2}. In between H_{C1} and H_{C2}, the line splitting is absent. We observe $1/^{51}T_1 \sim T^{2.2}$ at H_{C1} and it becomes almost temperature independent at H_{C2}, signaling gapless excitations at these two QCPs. Our experiment reveals highly nontrivial critical behaviors of the system, and hence

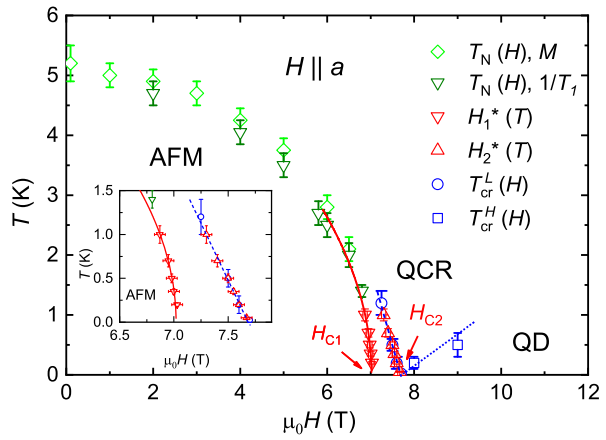

FIG. 1. Phase diagram of $SrCo_2V_2O_8$ in a transverse field along the a axis. AFM, QCR, and QD refer to the antiferromagnetic phase, the quantum critical regime, and the quantum disordered regime. Diamonds represent the Néel temperatures T_N determined by the magnetization data. Down triangles, circles, and squares represent T_N, the crossover temperatures T_{cr}^L and T_{cr}^H, respectively, all determined by the $1/^{51}T_1$ with different schemes of measurements (main text). The solid line is a function fit to $T_N \sim (H_{C1} - H)^{0.5}$ with $H_{C1} \approx 7.03$ T. The blue lines denote function fits to $T_{cr}^{L,H} \sim |H_{C2} - H|$ with $H_{C2} \approx 7.7$ T. Inset: An enlarged view of the fitting near the two QCPs.

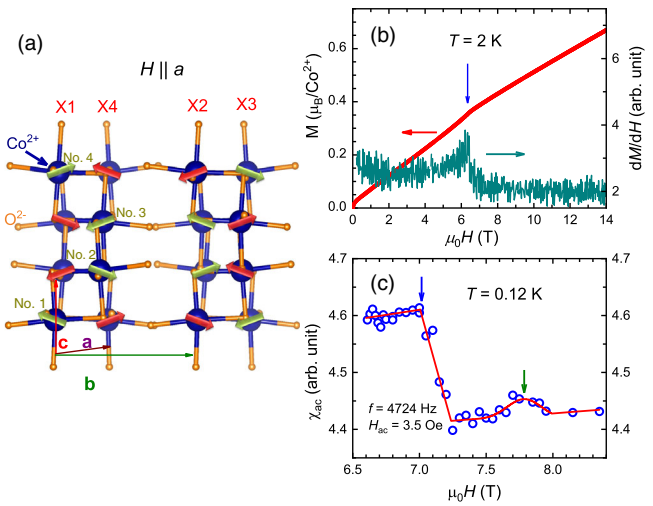

FIG. 2. (a) A schematic drawing of a unit cell of $SrCo_2V_2O_8$. a, b, and c label the tetragonal axes; $X1$ to $X4$ label four neighboring spin chains; No. 1 to No. 4 label the Co^{2+} sites along one screw chain. The arrows placed on the Co^{2+} sites mark the direction of the effective staggered field created by a dc field applied along the a axis. (b) The dc magnetization M vs H at 2 K and its derivative with the field. The arrow marks a peaked feature in dM/dH. (c) The ac susceptibility χ_{ac} as a function of H at 0.12 K. The arrows mark a sharp drop and a round peak in the data, respectively.

discovers a new route in accessing novel quantum criticality in quasi-1D Ising-like antiferromagnets, accomplished from screwed lattice structures.

The dc magnetization was measured above 2 K and the ac susceptibility was measured at 0.12 K. Details on sample preparation and NMR measuring techniques are described in Sec. S1 [31]. The ^{51}V ($I = 7/2$, $^{51}\gamma = 11.198$ MHz/T) NMR was performed in a dilution refrigerator with the spin-echo technique. The spin-lattice relaxation rate $1/^{51}T_1$ was measured by the inversion-recovery method, where the nuclear magnetization is well fit with the recovery function for $I = 7/2$ spins [32,33] without any stretching behavior, indicating the high quality of the sample (Sec. S8 [31]).

$SrCo_2V_2O_8$ crystalizes in a tetragonal space group $I4_1cd$ [17] as shown in Fig. 2(a). It consists of screwed chains along the c axis with alternative clockwise and anticlockwise screwing directions among neighboring chains [20]. Each unit cell contains four chain segments in the ab plane (labeled as $X1$ to $X4$), and each of them further includes four sites labeled as No. 1 to No. 4. Similar to $BaCo_2V_2O_8$, the primary interactions can be formulated as weakly coupled effective spin-1/2 antiferromagnetic XXZ chains with strong Ising anisotropy (Sec. S2 [31]). Because the vertical O—Co—O bond of $SrCo_2V_2O_8$ in the local CoO_6 octahedral tilts from the c axis by ~5.1° with a four-site period [34], the applied a axis transverse field H induces a two-period staggered field H_y and a four-period field H_z along the chain [23], as demonstrated in Fig. 2(a).

The applied and staggered fields suppress the antiferromagnetic Ising order [23], leading to a phase transition, signaled in our magnetization data. The Néel temperatures determined from the magnetization data at different fields (Sec. S3 [31]) are plotted in Fig. 1. At 2 K, the dc magnetization is shown as a function of field in Fig. 2(b), which exhibits a kinked feature at about 6.4 T. The dM/dH clearly resolves a peak at 6.4 T, consistent with a field-induced phase transition as reported earlier [17,20]. The ac susceptibility data at 0.12 K, as shown in Fig. 2(c), demonstrate a sharp drop at $\mu_0 H \approx 7$ T, indicating a quantum phase transition. In addition, we also observe a weak round peak at $\mu_0 H \approx 7.7$ T, indicating a crossover rather than a phase transition, which is a precursor to a 1D QCP and will be discussed in more detail later. In the following, we show unambiguous evidence for distinctive magnetic behaviors separated by 7 and 7.7 T by the ^{51}V NMR spectra and the spin-lattice relaxation rate $1/^{51}T_1$.

The ground state at each field can be identified by the NMR spectra at low temperatures. The ^{51}V spectra at frequencies close to $^{51}\gamma H$ are measured at typical fields and shown in Fig. 3(a). Three regimes are clearly seen. Below 7 T, the ^{51}V spectra have six peaks. Such a line splitting is caused by twinned magnetic domains in the Ising ordered phase originating from frustrated interchain exchange couplings [31,35,36], with an ordered moment of $1.81\mu_B$ per Co^{2+} [37]; In the intermediate field range from 7 to 7.7 T, a single NMR line is seen close to the central

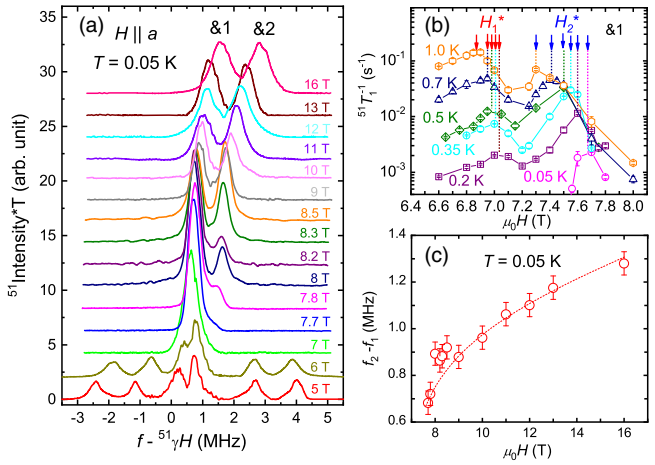

FIG. 3. (a) The ^{51}V NMR spectra measured at 0.05 K with typical fields. Escalated vertical offsets are applied for clarity. &1 and &2 mark the two resonance peaks at fields above 7.7 T. (b) The field dependence of $1/^{51}T_1$ at fixed temperatures measured on peak &1. H_1^* and H_2^* mark the field locations of peaked $1/^{51}T_1$ at each temperature. (c) The frequency difference between peak &1 and &2 as a function of field.

frequency $f \approx {}^{51}\gamma H$, which suggests the absence of magnetic ordering; At fields above 7.7 T, two NMR lines, labeled as &1 and &2, emerge and are resolvable at temperatures above 10 K (Fig. S8 [31]). The frequency difference of the two peaks increases with field [Fig. 3(c)], implying the system is paramagnetic when the field is above 7.7 T (Sec. S7 [31]).

The magnetic transition at each field can be resolved by $1/^{51}T_1$, which is measured at the primary peak of the spectra. In Figs. 4(a)–4(c), the $1/^{51}T_1$ with increasing temperature is shown at various fields. For fields below 6.5 T, a peak is observed in $1/^{51}T_1$, which determines the magnetic ordering temperature T_N. At 6.8 T, although a sharp drop of $1/T_1$ is not clearly discernible, the magnetic transition is resolved by a sudden drop of $1/^{51}T_1T$ at 1.35 K, as demonstrated in the inset of Fig. 4(a). For any fields above 7 T, no peaked feature in the $1/^{51}T_1$ is observed, indicating the absence of magnetic ordering. The determined T_N with the fields up to 6.8 T is shown in Fig. 1. It agrees well with T_N determined from our dc susceptibility data (Sec. S3 [31]).

To determine the transition precisely, we perform a field scan of $1/^{51}T_1$ at fixed T with increasing field, and the result is shown in Fig. 3(b). Surprisingly, at low temperatures the $1/^{51}T_1$ curve shows two prominent peaks with field. For instance, at 0.2 K, a low-field peak is located at ~7 T (marked as H_1^*), while a high-field one is at ~7.6 T (marked as H_2^*). These are close to the critical and the crossover field revealed in the ac susceptibility, respectively. We then plot $H_1^*(T)$ and $H_2^*(T)$ as functions of temperatures in the phase diagram of Fig. 1.

The $H_1^*(T)$ line, together with the high-temperature T_N data, portray the critical trajectory, which is well fit by $T_N \sim (H - H_{C1})^{\phi}$ with $H_{C1} = 7.03$ T and a critical exponent $\phi \approx 0.5 \pm 0.09$. Taking into account the absence of the NMR line splitting, the peaked feature in the $1/^{51}T_1(H)$, the sharp drop of χ_{ac}, and the mean-field-like exponent $\phi \approx 0.5$, all emerge at the same field $H_{C1} \approx 7$ T, we conclude that H_{C1} is a $(3+1)$D Ising critical point.

The determined T-H curve from $H_2^*(T)$ follows a straight line (Fig. 1). Given that no singularity of any thermodynamic quantity was observed, we understand it as a crossover approaching to a 1D QCP at $H_{C2} \approx 7.7$ T. This H_{C2} is also consistently resolved by the temperature evolution of $1/^{51}T_1$ data at different fields (Fig. 4). For fields either below or above H_{C2}, upon warming, the $1/^{51}T_1$ increases rapidly, and then crosses over to a weakly temperature-dependent behavior. This clearly indicates a gapped behavior below the crossover temperature T_{cr}^L (for $H < H_{C2}$) or T_{cr}^H (for $H > H_{C2}$) [Figs. 4(b) and 4(c)]. T_{cr}^L decreases with field, while T_{cr}^H increases with field. Interestingly, T_{cr}^L overlaps with the crossover line $H_2^*(T)$ in the studied temperature regime (Fig. 1). It scales linearly

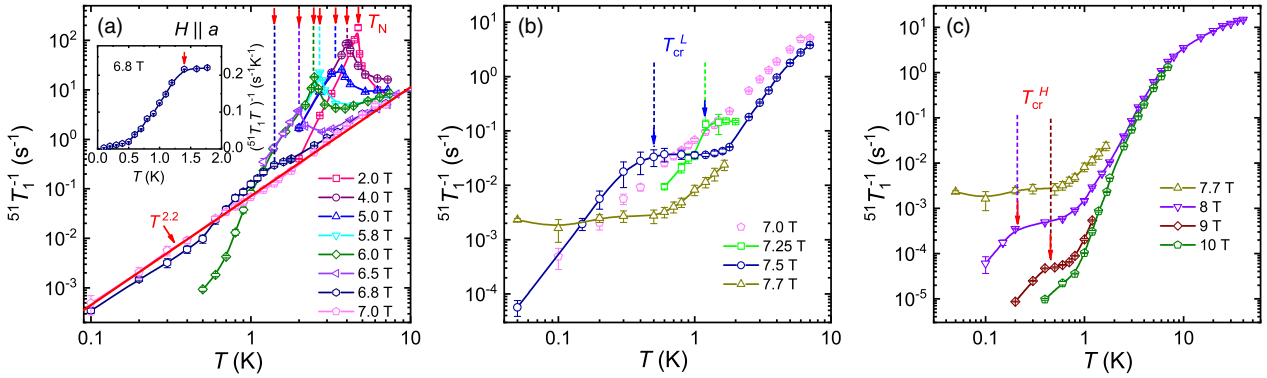

FIG. 4. The spin-lattice relaxation rate $1/^{51}T_1$ as functions of temperatures at various fields. (a) Data at fields below 7 T. The red arrows mark the peaked feature at T_N. The red straight line is a power-law function fit to the data at 7 T with $1/T_1 \sim T^{\alpha}$ ($\alpha = 2.2$). Inset: T_N at 6.8 T resolved by a sharp drop of $1/^{51}T_1T$ upon cooling. (b) Data at fields from 7 to 7.7 T. (c) Data at fields above 7.7 T. T_{cr}^L (T_{cr}^H) at each field marks a crossover temperature between a gapped and a gapless behavior.

with field by $T_{\rm cr}^{L} \sim |H - H_{C2}|$, implying the critical exponents $\nu z = 1$, consistent with the 1DTFIM universality class [2].

In the following, we show how the transitions at these two QCPs are affected by the induced staggered fields. First, the existence of a 1D QCP at a low field is further supported by our theoretical calculation. We model the primary interactions of $SrCo_2V_2O_8$ to a spin-1/2 Heisenberg-Ising chain, and the effective Hamiltonian reads as

$$H = \sum_i J[S_i^x S_{i+1}^x + S_i^y S_{i+1}^y + \Delta S_i^z S_{i+1}^z] - \mu_B g_x \sum_i \{H S_i^x + H_y (-1)^i S_i^y + H_z S_i^z \cos[\pi(2i-1)/4]\}, \quad (1)$$

with $J \approx 3.7$ meV and the anisotropic factor $\Delta \approx 2.1$ [20,23,27,38]. Here, g_x is the gyromagnetic ratio, H is the applied field along the a axis, H_y and H_z are, respectively, induced two- and four-period staggered fields along the b and c axes, due to screwed lattice structures [23]. By fitting the high-field magnetization data [39], we deduced $g_x \approx 3.7$, $H_y \approx 0.29\,H$, and $H_z \approx 0.14\,H$. We then apply the infinite time evolving block decimation (ITEBD) method [40] to determine the local static moment with respect to the field at zero temperature, shown in Sec. S4 [31]. The long-range antiferromagnetic order is continuously suppressed to zero at $H_C \approx 7.6$ T. Note that the calculated H_C value is very close to the measured H_{C2}. Compared to $H\|[110]$, the H_C for $H\|[100]$ is largely reduced [34]. This is primarily caused by the induced staggered field H_y, which is the strongest for $H\|[100]$ and tuned down to zero for $H\|[110]$ [34], consistent with the theoretical model [23].

Second, the scaling of the order parameter at H_C from the ITEBD calculation finds the critical exponent $\beta \approx 1/8$ (Fig. S6 [31]). This indicates that though H_C can be substantially reduced by the staggered field H_y, the QCP is still governed by the 1DTFIM universality [30,31] as described above.

Last, in quasi-1D systems, the locations of 1D and 3D QCPs reflect the competition between the effective interchain couplings and the external and induced fields, and are usually strongly material dependent. For example, the 1D QCP of $CoNb_2O_6$ is hidden inside a magnetically ordered phase close to a 3D QCP [13]. In $BaCo_2V_2O_8$ with a transverse field applied along the [110] direction, a 3D QCP is located at about 20 T, succeeded by a 1D QCP at about 40 T [28]. For $SrCo_2V_2O_8$, given its similar structural and magnetic properties to $BaCo_2V_2O_8$, two QCPs with field along the [110] direction are expected although not explored. By rotating the field from the [110] to the [100] direction, the induced staggered field might significantly lower both QCPs, and our measurements unambiguously show that the 1D QCP is outside the 3D ordered phase, yet are separated by a small field of 0.7 T.

The observation of the 1D QCP outside the 3D ordered phase prompts that the effective interchain couplings are very weak. This is likely caused by the heavy frustration among the interchain couplings [20,27]. The induced staggered fields, which are tied up with the screwed structure, may further enhance the frustration effects and help weaken the 3D order. However, a full discussion on this would need detailed information on the interchain couplings, which is beyond the scope of this Letter.

In what follows, we discuss the spin dynamics at both the 1D and 3D QCPs. As for the 3D QCP at H_{C1}, our $1/^{51}T_1$ data exhibit a power-law scaling $1/^{51}T_1 \sim T^{2.2}$ from 10 K down to 0.1 K [Fig. 4(a)]. Such a power-law scaling over two decades of temperatures evidences gapless excitations at H_{C1}. At the 1D QCP, H_{C2}, the $1/^{51}T_1$ stays nearly constant, for over one decade in temperature below 0.5 K, which also evidences gapless excitations. The 1DTFIM predicts $1/T_1 \sim T^{-0.75}$ at the QCP [13], while we observe a weakly T-dependent $1/T_1$ at H_{C2}. The deviation may arise if our measurement missed the exact H_{C2}, or if the temperature is not low enough. It is worth noting that for fields just below H_{C2}, the rapid drop of $1/T_1$ with decreasing temperature signals gapped excitations. This agrees with the prediction in the 1DTFIM, and to our knowledge, such a gap opening behavior has never been reported before.

We draw connections between our observations and the proposed topological phase transitions in $BaCo_2V_2O_8$ [26]. The induced two-period staggered moments have been verified by the neutron scattering study on $BaCo_2V_2O_8$ [26]. We expect that they also appear in $SrCo_2V_2O_8$, given their similar lattice and magnetic structures [20]. More evidence comes from the lower critical field along the [100] direction in $SrCo_2V_2O_8$, which is consistent with a stronger induced staggered field by the larger tilt angle of the O—Co—O bond in this compound [34]. Although the materials are slightly different, the properties, especially the gapped excitations, in both the ordered phase at $H \ll H_C$ and the paramagnetic phase at $H \gg H_C$, are the same. However, when the 1D QCP is outside the 3D ordered phase, as in the case of $SrCo_2V_2O_8$, gapless excitations emerge at the two QCPs, since static linear confining potential is absent above H_{C1}. Moreover, an exposed 1D QCP outside the 3D ordered phase at a relatively low field promises an ideal approach for experimental investigation of the genuine 1D quantum criticality. For future studies, by rotating the field from [100] to [110] direction, two QCPs may be further separated. This is indeed recently proved theoretically [41].

In summary, our NMR study on $SrCo_2V_2O_8$ reveals two separated quantum critical points experimentally with a transverse field, for the first time in this material. Our results also demonstrate distinctive quantum critical

behaviors at the two QCPs, including the scaling behaviors of the transition and crossover temperatures and the spin dynamics. We propose that separate 1D and 3D QCPs are realized at very low fields, attributed to novel effects of the effective staggered magnetic field. Such a one-dimensional quantum critical point exposed outside the three-dimensional magnetic ordered phase at a low magnetic field opens a new avenue to access the genuine quantum criticality of the one-dimensional transverse-field Ising model experimentally.

The authors acknowledge discussions with Prof. Bruce Normand. This work is supported by the Ministry of Science and Technology of China (Grants No. 2016YFA0300504 and No. 2016YFA0300503), the National Natural Science Foundation of China (Grants No. 51872328, No. 21875249, No. 11674392, No. U1632159, and No. 11804221), the Fundamental Research Funds for the Central Universities, the Research Funds of Renmin University of China (Grant No. 18XNLG24), the Science and Technology Commission of Shanghai Municipality Grant No. 16DZ226020, and the Outstanding Innovative Talents Cultivation Funded Programs of Renmin University of China. J. W. acknowledges additional support from a Shanghai talent program.

*hezz@fjirsm.ac.cn
†wujd@sjtu.edu.cn
‡wqyu_phy@ruc.edu.cn

[1] H. V. Loehneysen, J. Low Temp. Phys. **161**, 1 (2010).
[2] S. Sachdev, *Quantum Phase Transitions* (Cambridge University Press, Cambridge, England, 2011).
[3] P. Coleman and A. J. Schofield, Nature (London) **433**, 226 (2005).
[4] P. Pfeuty, Ann. Phys. (N.Y.) **57**, 79 (1970).
[5] E. Barouch and B. M. McCoy, Phys. Rev. A **3**, 786 (1971).
[6] R. Jullien, P. Pfeuty, J. N. Fields, and S. Doniach, Phys. Rev. B **18**, 3568 (1978).
[7] J. H. H. Perk, H. W. Capel, G. R. W. Quispel, and F. W. Nijhoff, Physica (Amsterdam) **123A**, 1 (1984).
[8] A. B. Zamolodchikov, Int. J. Mod. Phys. A **04**, 4235 (1989).
[9] S. T. Carr and A. M. Tsvelik, Phys. Rev. Lett. **90**, 177206 (2003).
[10] J. H. H. Perk and H. Au-Yang, J. Stat. Phys. **135**, 599 (2009).
[11] J. Wu, M. Kormos, and Q. Si, Phys. Rev. Lett. **113**, 247201 (2014).
[12] J. Wu, L. Zhu, and Q. Si, Phys. Rev. B **97**, 245127 (2018).
[13] A. W. Kinross, M. Fu, T. J. Munsie, H. A. Dabkowska, G. M. Luke, S. Sachdev, and T. Imai, Phys. Rev. X **4**, 031008 (2014).
[14] R. Coldea, D. Tennant, E. Wheeler, E. Wawrzynska, D. Prabhakaran, M. Telling, K. Habicht, P. Smeibidl, and K. Kiefer, Science **327**, 177 (2010).
[15] S. Lee, R. K. Kaul, and L. Balents, Nat. Phys. **6**, 702 (2010).
[16] Z. He, T. Taniyama, T. Kyomen, and M. Itoh, Phys. Rev. B **72**, 172403 (2005).
[17] Z. He, T. Taniyama, and M. Itoh, Phys. Rev. B **73**, 212406 (2006).
[18] S. Kimura, H. Yashiro, K. Okunishi, M. Hagiwara, Z. He, K. Kindo, T. Taniyama, and M. Itoh, Phys. Rev. Lett. **99**, 087602 (2007).
[19] A. K. Bera, B. Lake, F. H. L. Essler, L. Vanderstraeten, C. Hubig, U. Schollwöck, A. T. M. N. Islam, A. Schneidewind, and D. L. Quintero-Castro, Phys. Rev. B **96**, 054423 (2017).
[20] A. K. Bera, B. Lake, W.-D. Stein, and S. Zander, Phys. Rev. B **89**, 094402 (2014).
[21] S. Kimura, T. Takeuchi, K. Okunishi, M. Hagiwara, Z. He, K. Kindo, T. Taniyama, and M. Itoh, Phys. Rev. Lett. **100**, 057202 (2008).
[22] M. Klanjšek, M. Horvatić, S. Krämer, S. Mukhopadhyay, H. Mayaffre, C. Berthier, E. Canévet, B. Grenier, P. Lejay, and E. Orignac, Phys. Rev. B **92**, 060408(R) (2015).
[23] S. Kimura, K. Okunishi, M. Hagiwara, K. Kindo, Z. He, T. Taniyama, M. Itoh, K. Koyama, and K. Watanabe, J. Phys. Soc. Jpn. **82**, 033706 (2013).
[24] S. K. Niesen, G. Kolland, M. Seher, O. Breunig, M. Valldor, M. Braden, B. Grenier, and T. Lorenz, Phys. Rev. B **87**, 224413 (2013).
[25] A. Okutani, S. Kimura, T. Takeuchi, and M. Hagiwara, Appl. Magn. Reson. **46**, 1003 (2015).
[26] Q. Faure, S. Takayoshi, S. Petit, V. Simonet, S. Raymond, L. Regnault, M. Boehm, J. S. White, M. Månsson, C. Rüegg, P. Lejay, B. Canals, T. Lorenz, S. C. Furuya, T. Giamarchi, and B Grenier, Nat. Phys. **14**, 716 (2018).
[27] Z. Wang, J. Wu, S. Xu, W. Yang, C. Wu, A. K. Bera, A. T. M. Nazmul Islam, B. Lake, D. Kamenskyi, P. Gogoi, H. Engelkamp, N. Wang, J. Deisenhofer, and A. Loidl, Phys. Rev. B **94**, 125130 (2016).
[28] Z. Wang, T. Lorenz, D. I. Gorbunov, P. T. Cong, Y. Kohama, S. Niesen, O. Breunig, J. Engelmayer, A. Herman, Jianda Wu, K. Kindo, J. Wosnitza, S. Zherlitsyn, and A. Loidl, Phys. Rev. Lett. **120**, 207205 (2018).
[29] M. Matsuda, H. Onishi, A. Okutani, J. Ma, H. Agrawal, T. Hong, D. M. Pajerowski, J. R. D. Copley, K. Okunishi, M. Mori, S. Kimura, and M. Hagiwara, Phys. Rev. B **96**, 024439 (2017).
[30] S. Takayoshi, S. C. Furuya, and T. Giamarchi, Phys. Rev. B **98**, 184429 (2018).
[31] See Supplemental Material at http://link.aps.org/supplemental/10.1103/PhysRevLett.123.067203 for the crystal information, dc magnetization data, the ITEBD results, the NMR line shape discussions, and typical spin recovery curves.
[32] D. E. MacLaughlin, J. D. Williamson, and J. Butterworth, Phys. Rev. B **4**, 60 (1971).
[33] S. Wada, R. Aoki, and O. Fujita, J. Phys. F **14**, 1515 (1984).
[34] S. K. Niesen, O. Breunig, S. Salm, M. Seher, M. Valldor, P. Warzanowski, and T. Lorenz, Phys. Rev. B **90**, 104419 (2014).
[35] Y. Kawasaki, Y. Ideta, Y. Kishimoto, T. Ohno, K. Omura, T. Fujita, S. Kimura, and M. Hagiwara, J. Phys. Soc. Jpn. **3**, 014001 (2014).
[36] J. Liu, J. Wang, W. Luo, J. Sheng, Z. He, S. A. Danilkin, and W. Bao, Chin. Phys. Lett. **33**, 037502 (2016).

[37] L. Shen, O. Zaharko, J. O. Birk, E. Jellyman, Z. He, and E. Blackburn, New J. Phys. **21**, 073014 (2019).
[38] Z. Wang, M. Schmidt, A. K. Bera, A. T. M. N. Islam, B. Lake, A. Loidl, and J. Deisenhofer, Phys. Rev. B **91**, 140404(R) (2015).
[39] A. Okutani, T. Kida, T. Usui, T. Kimura, K. Okunishi, and M. Hagiwara, Phys. Procedia **75**, 779 (2015).
[40] R. Orús and G. Vidal, Phys. Rev. B **78**, 155117 (2008).
[41] H. Zou, R. Yu, and J. Wu, arXiv:1904.11398.